Current Research in Food Science 4 (2021) 784–799

Contents lists available at ScienceDirect

Current Research in Food Science

journal homepage: www.sciencedirect.com/journal/current-research-in-food-science

Research Paper

Effect of different derivatives of paraffin waxes on crystallization of eutectic mixture of cocoa butter-coconut oil

Bhagyashri L. Joshi *, Robert Graf, Sarah Gindra, Thomas A. Vilgis **

Max-Planck-Institute of Polymer Research, Mainz, Germany

ARTICLE INFO

Keywords:
Paraffin wax
Thermal behavior
Ternary state diagram
Crystallization kinetics
Rheology
Rheo-microscopy

ABSTRACT

Paraffin wax is a mixture of numerous unbranched hydrocarbons used frequently for various purposes: to improve the shelf life of products containing lipid system and develop more shiny products. However, because of its complex nature, the effect of such molecular structure on the solid phase behavior of lipids is hardly unstated. Hence in our study, we focus on understanding the impact of derivatives of paraffin wax on the lipid system. In the current work, three unbranched derivatives of paraffin wax: Eicosane C (20), Pentacosane C (25) and Triacontane C (30) were selected as additives. These n-alkanes are specifically added to the eutectic mixture of cocoa butter (CB) and coconut oil (CO) ($E_{CB\text{-}CO}$) to observe the effect on thermal, morphological, rheological properties and crystallization kinetics with respect to the carbon chain length. Results from our study illustrate that melting and crystallization temperature, storage modulus and solid fat content (SFC) increases after the addition of 1 wt% of C (20), C (25). In contrast, there is a phase separation for 1 wt% C (30). Further similar study with addition of n-alkanes to pure CB and CO reveals that the interaction of n-alkanes with $E_{CB\text{-}CO}$ is dominated by the interaction of n-alkanes with CO instead of CB. Therefore, our findings provide insight into the effect of addition of n-alkanes having different carbon chain length and their respective concentration on crystallization process of CB and CO. This will definitely help to design the processes for products containing such model systems.

1. Introduction

Crystallization modifiers are used to alter systematically the crystallization processes and temperature of lipid systems. For instance, the modifiers like monoacylglycerol (MAG), sorbitan esters (SEs), sucrose esters of fatty acids (SEFAs), lecithin and polyglycerol polyricinoleate (PGPR) can be used to tailor the physical characteristics of the lipid based systems (Ribeiro et al., 2015). Due to their chemical structure as a combination of hydrophilic and hydrophobic parts, they can emulsify, stabilize, and help to modify solid phase behavior of food products (Miskandar et al., 2007; Tran et al., 2015). The extensive use of these modifiers to lipid crystallization has been widely explored; however, a new trend of modifiers such as natural waxes is in wide use to increase the shelf life and a coating agent to fruits and vegetables (Zhang et al., 2017). Such usage of waxes recently seized attention towards tailoring the crystallization processes in a controlled way.

Waxes are usually complex mixtures of various constituents as hydrocarbons, wax esters, phenolic esters, fatty alcohols, mono-, di- and triacylglycerols etc. (Sato, 2018). Therefore, due to the presence of a hydrophobic part as long alkyl chain in waxes, the possibility to modify the crystallization of triacylglycerol (TAG) in fats after mixing them together is significant (Martini et al., 2008). Waxes are further categorized into natural waxes such as candelilla wax, rice bran wax, beeswax, etc. and petroleum waxes: paraffin wax, microcrystalline wax, etc. The blend of oil and natural waxes shows similar physico-chemical properties as saturated fats but are usually non-digestible; hence, it can be used as saturated fat replacers in many applications (Blake et al., 2014; Zulim Botega et al., 2013). These combinations of oil with wax tend to form oleogel and hence waxes are also known as organo-gelator. Because of such novel characteristics, wide applications in the food, cosmetics and pharmaceutical industries are possible and easy to control. Therefore, in our study, paraffin wax as an additive was selected to understand the

Abbreviations: CB, Cocoa Butter; CO, Coconut Oil; $E_{CB\text{-}CO}$, Eutectic mixture of CB and CO; SFC, Solid Fat Content; DSC, Differential Scanning Calorimetry; PLM, Polarized Light Microscopy; NMR, Nuclear Magnetic Resonance; LMOGs, Low Molecular Weight Organogelators; HMF, High Melting Fraction.

* Corresponding author.
** Corresponding author. Ackermannweg 10, 55128 Mainz, Germany.
E-mail addresses: joshi@mpip-mainz.mpg.de (B.L. Joshi), vilgis@mpip-mainz.mpg.de (T.A. Vilgis).

https://doi.org/10.1016/j.crfs.2021.10.010
Received 17 May 2021; Received in revised form 26 October 2021; Accepted 26 October 2021
Available online 2 November 2021

effect on crystallization of $E_{CB\text{-}CO}$. It mainly consists of mixtures of straight-chain hydrocarbon, ranging from 18 to 30 (Freund et al., 1983). The general use of paraffin wax (food grade) in chocolate production is to provide a shiny appearance and increase the melting temperature of chocolate (Filippone, 2019). Even though one of the uses has already been established, the interaction of this wax with TAGs from CB and CO is yet to understand. In this current study, only pure derivatives of this wax has been considered for better elucidating of the interaction. Three different derivatives of paraffin wax: Eicosane C (20); Pentacosane C (25) and Triacontane C (30), with melting temperature of 37 °C, 56 °C and 66 °C were used.

Cocoa butter (CB) is the most important component in chocolate production, responsible for different characteristics of the final product quality, such as complete melting in the mouth, hardness, brightness, snap at room temperature, etc. Moreover, CB represents the most expensive fraction of the cost of the material (~25–36% of end product) in the manufacturing of chocolates (Ribeiro et al., 2015). Therefore, to understand the behavior of CB, its constituents are essential to distinguish. CB consists of mainly monounsaturated symmetrical triacylglycerol (TAG), namely POP (1,3-dipalmitoyl-2-oleoyl glycerol), POS (1,3-palmitoyl-stearoyl-2-oleoyl glycerol) and SOS (1,3-distearoyl-2-oleoyl glycerol); where P = palmitic acid, O = oleic acid and S = stearic acid (approximately 17% of POP, 37% of POS and 27% of SOS) (Loisel et al., 1998). The remaining part consists of mixtures of mono-unsaturated and TAGs composed of FA of different chain lengths (Joshi et al., 2020) and traces of polyphenols and free fatty acids. Due to the presence of wide ranges of TAGs, the crystallization of CB involves polymorphism. CB crystallizes into (γ, α, β_2', β_1', β_2 and β_1) different polymorphs in which melting temperature and their stability increases from γ (17.3 °C) to β_1 (36.3 °C) (Wille and Lutton, 1966). Hence, to summarize, the production of good quality chocolate is controlled by the precise tailoring of the crystal phases of CB, which is ultimately associated with the processing and favorable storage conditions. However, the costs associated with CB crystallization are still challenging factors for many industrial sectors. Therefore, cocoa butter substitutes, replacers and addition of modifiers to the CB while processing measures, are to be added to modify the crystallization and eventually reduce costs of processing or robustness of polymorph.

One of the cocoa butter substitutes in the confectionery industry is Coconut Oil (CO) (Lipp and Anklam, 1998). It consists of a high amount of saturated fatty acids (~90%), with the remainder being mono-unsaturated and polyunsaturated fatty acids. The TAG composition in CO is of various mixed saturated fatty acids, as - MLaLa, LaLaLa, MMLa, PMLa; where M - Mystric acid C (14:0), La - Lauric acid C (12:0), and P - Palmitic acid C (16:0), but mainly consists of lauric acid (~40%) (Rothkopf and Danzl, 2015). After crystallization, these TAGs form polymorphs of α and β' crystalline structure and their melting temperature is very close to the melting temperature of CB (Jahurul et al., 2014). A wide range of research studies have been done previously on mixing behavior and crystallization of CB with lauric fats (Ali and Dimick, 1994; Geary and Hartel, 2017; Quast et al., 2013; Williams et al., 1997). Recently, we explored the effect of isothermal and dynamic crystallization processes on physicochemical properties and morphological changes of a broad range of CB/CO blends. (Joshi et al., 2020). There we have shown that CB/CO blends tend to form a eutectic mixture at 65 wt% of CO and 35 wt% of CB ($E_{CB\text{-}CO}$). Thus, this result led to an innovative idea of using derivatives of n-alkanes as a modifier in the eutectic mixture for further development of crystallization, for instance, less demixing, which leads to better co-crystallization.

In the present study, we, therefore, prepared a unique proposition for modifying the crystallization of $E_{CB\text{-}CO,}$ shedding light on 1) the physical aspect of pseudo ternary mixing behavior and 2) effect of n-alkanes on mobile phase (liquid fraction remained after crystallization) of $E_{CB\text{-}CO}$ implying oleogel formation as similar to usual oleogels from oil and wax mixture. In order to evaluate these aspects, the study was carried out by understanding the effect of the addition of n-alkanes into $E_{CB\text{-}CO}$ on mixtures' thermal, morphological, mechanical properties, along with understanding the effect on crystallization kinetics with respect to a carbon chain length of n-alkanes. The study evaluates the occurrence of possible interactions for variations in thermal and mechanical properties after the addition of C (20), C (25) and C (30). Using this data, we predict the ternary plot with melting temperature projections.

2. Material and method

2.1. Materials and blends preparation

CB (Carl Roth GmbH + Co. KG, Germany), CO (Sigma-Aldrich GmbH, Germany), C (20), C (30) (Alfa Aesar) and C (25) (MP Biomedicals, LLC) were used as a model system. For the preparation of samples, CB and n-alkanes and CO were heated individually for 15 min at 90 °C and then molten form of fats are added together; this mixture was further heated for 30 min more at 90 °C while stirring with the speed of 200 rpm. Later, the mixture was transferred into a preheated sample holder (e.g. aluminum crucible for DSC). Afterwards, the sample was heated again for 15 min in the oven to eliminate the crystallization due to temperature difference while transferring the sample. After preparing the sample, it was stored for 24 h at 22 °C in a constant climate chamber (Binder KMF115) with 0% relative humidity prior to all DSC and PLM experiments. For crystallization kinetics studies, after heating to 90 °C, the sample was moved to sample holders of NMR and rheometer and experiments had started immediately.

2.2. Thermal characteristics

DSC was used for the thermal analysis of mixtures. The blends were prepared as explained in section 2.1 and then stored in an aluminum crucible (~10 mg–20 mg sample) for 24 h at 22 °C prior to DSC (Mettler Toledo DSC3+/700/453) measurements. An empty 100 μL Aluminum pan was considered as a reference cell. Liquid nitrogen was used for cooling at a rate of 30 mL/min. The experiment was performed in four segments to study the thermal properties of $E_{CB\text{-}CO}$ after adding n-alkanes via isothermal and dynamic processes. The sample, which was crystallized by the isothermal process at 22 °C, heated firstly to 90 °C to study the crystal formation after 24 h and kept for 20 min for erasing all crystal memory. Later, the sample was cooled to −50 °C and immediately heated to 90 °C in the next segment. Here, we have considered the peak temperature as the melting/crystallization temperature of the system and onset and offset point denotes the start and end of the thermal process. To better understand the DSC profile, the heat flow parameter is increased in steps of 0.2 W/g in each sample measurement while plotting in section 3.2. The analysis was performed in triplicates and the evaluation of the graphs was carried out in STARe software. Furthermore, the ternary plot was constructed by using OriginPro software to understand the melting behavior for ternary mixing of CB-CO and n-alkanes.

2.3. Morphological studies

The morphology of the samples was studied by PLM (Zeiss Scope. A1 Pol). 10 μL of the sample was pipetted to a preheated microscope slide and carefully, the coverslip was placed on the top of the molten sample to avoid air bubble formation. These slides were stored at 22 °C for 24 h prior to PLM. The pictures were captured after 24 h for each sample and the result of dynamic crystallization was studied by using a temperature profile similar to the one used in DSC analysis. The heating and cooling were attained by a Peltier plate setup (Linkam, model PE120). The sample was heated to 90 °C with a 2 K/min rate and kept isothermally for 60 min to erase the crystal memory. As the heating systems are different in DSC and PLM, longer isothermal heating time at 90 °C was used as compared to DSC. Afterwards, the sample was cooled down to 10 °C with a 2 K/min rate and at this temperature, the pictures were

captured by using objectives 10 and 20x. All measurements were carried out in duplicates.

2.4. Solid fat content (SFC) analysis

To understand the effect of the addition of n-alkanes having different chain lengths on crystallization kinetics of $E_{CB\text{-}CO}$ in terms of SFC (%), ^1H solid-state nuclear magnetic resonance (NMR) was performed on the samples. The NMR experiments were accomplished with a Bruker Avance III console operating at 500.22 MHz ^1H Larmor frequency at a Bruker superconducting 11.9 T wide bore magnet system using a commercial static $^1H/X$ static solid-state NMR probe. Spherical sample shape was chosen using 4 mm HR-MAS rotors as sample holder, in order to reduce susceptibility artifacts. The ^1H rf nutation frequency was adjusted to 62.5 kHz, corresponding to a 90° pulse length of 4 μs. The temperature was adjusted using a Bruker BSVT temperature controller with an accuracy of ± 0.1 K calibrated using the temperature-dependent chemical shifts of methanol and ethylene glycol.

The blends were prepared as explained in section 2.1 and then transferred to the preheated sample holder of NMR. The probe and the sample holder of the machine have been preheated to 90 °C prior to experiments. The sample was cooled from 90 °C to 22 °C at a rate of 0.5 K/min rate. The cooling rate has been selected to maintain the system as equilibrium as possible. After reaching 22 °C, the sample was kept for 24 h in order to monitor the crystallization kinetics. The automated program was set to take a spectrum after every 15 min of the timeline. Each crystallization experiment was performed in duplicates.

In order to calculate the SFC, the spectra were further analyzed. The liquid sample is detected as a sharp peak while the broad signal indicates the solid sample, as shown in supplementary figure S1. Hence for calculating the SFC, the following equation was used.

$$\boldsymbol{SFC}\ (\%) = \frac{(\boldsymbol{A_{fs}} - \boldsymbol{A_{sp}})}{\boldsymbol{A_{fs}}} * 100 \tag{1}$$

A_{sp} = Integrated area under the sharp peak
A_{fs} = Integrated area under the full spectrum

SFC for all the spectra was calculated by using MATLAB automated program.

Furthermore, the relation of SFC vs. time was analyzed by using the Avrami model in order to understand the crystallization kinetics in detail. This model is being used to measure crystallization kinetics and understand the nature of the crystal growth process (Avrami, 1939, 1940, 1941). In order to represent this model in terms of time-dependent SFC in fat crystallization, equation (2) was used-

$$\frac{\boldsymbol{SFC(t)} - \boldsymbol{SFC(0)}}{\boldsymbol{SFC(max)\ or\ SFC(\infty)} - \boldsymbol{SFC(0)}} = \left(1 - \boldsymbol{e}^{-kt^n}\right) \tag{2}$$

Where, $SFC(t)$ is the solid fat content at a particular time t; $SFC(max)$ is the maximum SFC achieved at a specific temperature or equilibrium solid fat content $SFC(\infty)$ and $SFC(0)$ is the SFC at time t = 0 (Marangoni and Wesdorp, 2012). Ideally, $SFC(0)$equals zero as no crystals are formed, however, in our case at 22 °C already some amount of solids were detected hence the eq. (2) was used as it is. The Avrami parameter (k) is a function of crystallization temperature and considers the relation of nucleation and crystal growth rates altogether. Whereas the non-universal Avrami exponent (n) is a number that focus empirically on the crystal growth mechanism. This is a combination of function of time dependence of nucleation and the number of dimensions in which growth takes place.

2.5. Mechanical properties

To measure the effect on the viscoelastic properties of $E_{CB\text{-}CO}$ after adding n-alkanes, 40 mm cross-hatched parallel plate geometry (Hybrid Discovery HR-3) was used. The sample was cooled from 90 °C to 22 °C with a cooling rate of 0.5 K/min with a strain of 0.01%. After reaching 22 °C, the time sweep was performed for 2 h and 30 min. This timeline was selected based on the primary results of crystallization kinetics under polarized light microscopy with the same approach to obtain a well-developed crystal network for additional analysis. To further characterize the sample, amplitude sweep was carried out from the range of strain 0.001–100% to understand the crystal network's strength. From these data, the Linear Viscoelastic (LVE) and non-Linear Viscoelastic (NLVE) regimes were determined based on each different composition. The experiments were performed in triplicates. The evaluation of graphs was carried out in origin software. The parameters used for the investigation are shown in Table 1.

2.6. Rheo-microscopy

In situ microscopy accessory was used to observe the crystal network formation under rheometer and understand the effect of oscillation strain on fat crystal network. For measurements, modifications in parameters were considered with respect to typical rheometer settings. The gap between the two plates was reduced by 10% than the non-optical cross-hatched plate assembly in order to observe clear images. 0.001% of the oscillation strain rate was used. 60 °C was considered as the start temperature instead of 90 °C due to limitations of the high-temperature resistance to microscope objectives. After reaching the plateau region, an amplitude sweep was carried out. The single video was captured during amplitude sweep as 'multipage tiff' with a 9 Hz frame rate. Captured videos showed crystals' 3D network connectivity arrangements in three layers: upper layer (at upper plate surface), middle and lower layer (at the bottom plate). 20x objective was used. The parameters used for carrying out experiments are shown in Table 1. The resultant videos were analyzed by using Image J software. The color, brightness and contrast were manipulated by using Image J. The 'multipage tiff' file was converted into 'avi' file with a 14 fps rate. In total, 1776 frames were captured throughout amplitude sweep and the exact image was selected for representing the figure in the result section.

3. Result and discussion

3.1. Selection rule

This section illustrates the initial experimental results, which contributed to set the path for the current study. Initially, 1, 2, 3, and 5 wt% of C (20), C (25) and C (30) were added to $E_{CB\text{-}CO}$ for understanding the effect of different concentrations of n-alkanes on crystallization in terms of crystal morphology. The microscopy results (Fig. 1 (a)) show that after the addition of 1 wt% of C (20), the random aggregation of the small needle-like structure takes place. Further addition of 2, 3 and 5 wt % of C (20) indicates that these random aggregations of needle-like structures form spherulitic morphology. At this stage, we believe that

Table 1
Experimental parameters for rheology.

Parameters used for experiment	Rheometer values	Rheo-microscopy values
Start temperature	90 °C	60 °C
End temperature	22 °C	22 °C
Soak time at 90/60 °C	15 min	15 min
Cooling ramp	0.5 K/min	0.5 K/min
Strain (%)	0.01	0.01
Axial force	0 N	0 N
Frequency	1 Hz	1 Hz
Torque	100000 μN m	100000 μN m
Gap	1000 μm	100 μm
Geometry	Cross-hatched parallel plate 40 mm ø	Smooth parallel plate 40 mm ø

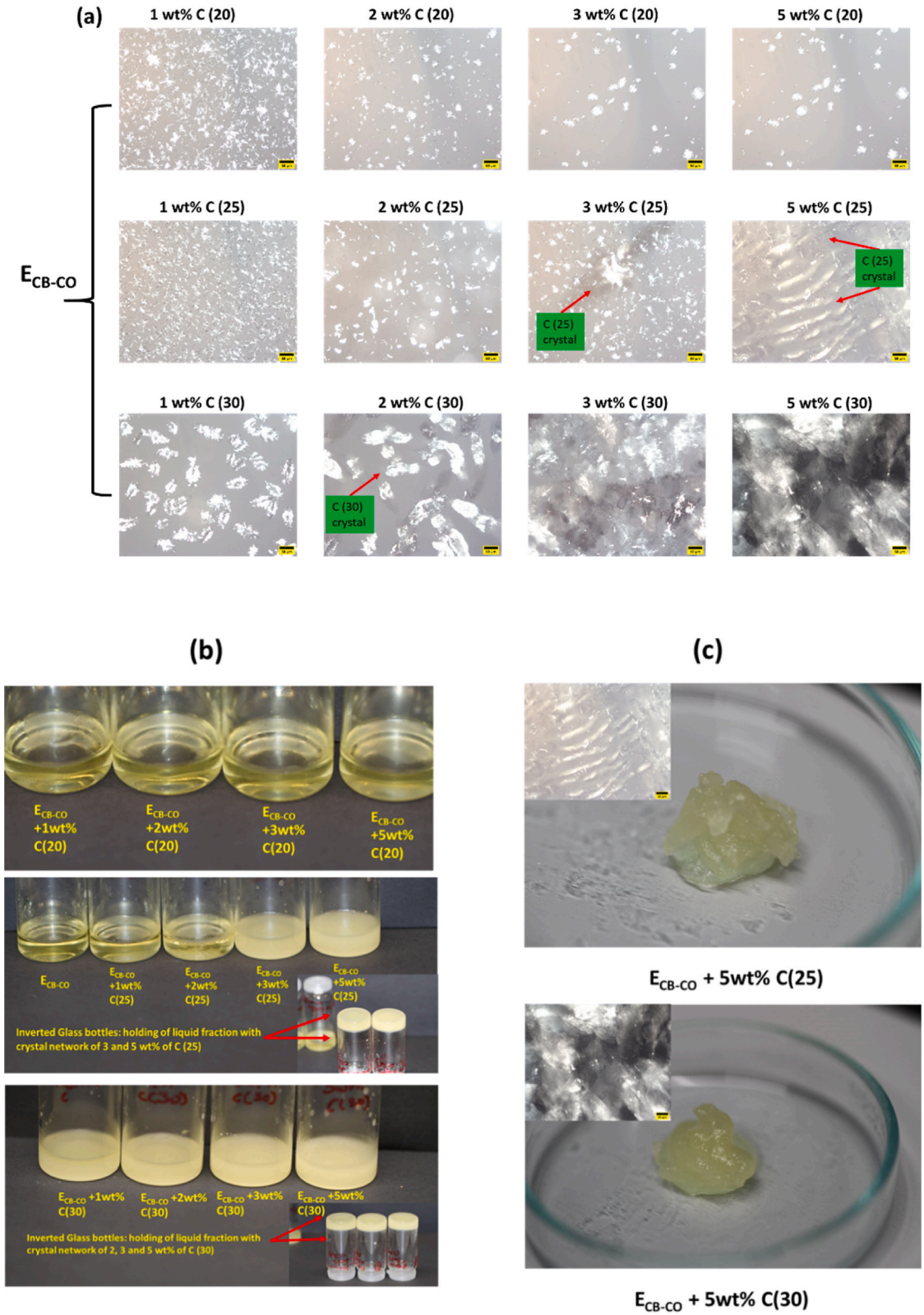

Fig. 1. (a): Microscopic representation of changes in morphology with respect to addition of 1, 2, 3 and 5 wt% of C (20), C (25) and C (30) in $E_{CB\text{-}CO}$. 3 and 5 wt% of C (25) and all C (30) addition shows two different morphologies, which is shown with red arrow. The scale bar represents 50 μm. (b) The glass bottles representing the macroscopic view of pure $E_{CB\text{-}CO}$ and its comparison with 1, 2, 3 and 5 wt% of C (20), C (25) and C (30) addition after 24 h at 22 °C. Inset reveals that inversion of glass bottles for 3 and 5 wt% of C (25) and 2,3 and 5 wt% of C (30) sample, holds the liquid fraction of $E_{CB\text{-}CO}$. This indicates oleogel-like property. (c) An example for oleogel-like property after addition of 5 wt% of C (25) and C (30). Inset represents the microscopic view of gels. (For interpretation of the references to color in this figure legend, the reader is referred to the Web version of this article.)

a larger percentage of C (20) results in a lower number of crystals with large and defined crystal size and shape. Similar results are observed in case of 1 and 2 wt % of C (25); however, the 'fiber or rod-like' morphology (indicated with red arrow) is observed for 3 and 5 wt% of C (25) along with a small spherulitic structure formation. Further, the addition of 1 wt% of C (30) reveals that tiny crystals granules are situated at the surface of 'fiber like' structures. While, more addition of C (30) from 2 to 5 wt%, resulted in the formation of 'fiber like' to vague (unspecific) morphological structures respectively. Evidence from this primary study implies that two types of morphologies form in case of the addition of 3 and 5 wt% C (25) and for all concentrations of C (30) to $E_{CB\text{-}CO}$. Additionally, the effect on bulk samples of pure $E_{CB\text{-}CO}$ and its comparison with addition of 1, 2, 3 and 5 wt% of C (20), C (25) and C (30) reveals that, after 24 h at 22 °C, the samples with addition of C (20) crystallize as a thin layer on the surface of a liquid part. Similarly, a thin layer of crystals due to 1 and 2 wt% of C (25) is visible (Fig. 1 (b)). Whereas, the samples with 3 and 5 wt% of C (25) represent opaque mixture instead of transparent (as pure $E_{CB\text{-}CO}$ and samples with all concentrations of C (20), which are in transparent liquid state), which is the effect of crystallization of samples. Furthermore, the inverted position of these two glass bottles does not allow the liquid portion to flow by gravity. Similarly, in case of C (30) addition to $E_{CB\text{-}CO}$, all the samples show crystallization; however, only 2, 3 and 5 wt% of C (30) show the effect of holding the liquid fraction of $E_{CB\text{-}CO}$ against the pull of gravity. Therefore, micro and macroscopic point of view affirm that large quantity of $E_{CB\text{-}CO}$ prefers to stay in a liquid state at 22 °C after 24 h, while crystals of 3 and 5 wt% of C (25) and 2, 3 and 5 wt% of C (30), act as a network, which entraps the liquid fraction of $E_{CB\text{-}CO}$. This behavior resembles 'oleogel-like' properties. An oleogel can be defined as an organic liquid entrapped within a thermoreversible three-dimensional gel network. This network is either to be formed by polymers or low molecular weight organo gelators (LMOGs) (Stortz et al., 2012). In our study, instead of only liquid fraction entrapment in three-dimensional network of LMOGs, the solid and liquid fraction of $E_{CB\text{-}CO}$ entrapped within the colloidal network of C (25) and C (30) with the strength sufficient to immobilize the liquids against the pull of gravity (Abdallah and Weiss, 2000). The 'oleogel-like' behavior is possible to visualize for 5 wt% of C (25) and C (30) addition, respectively (Fig. 1 (c)). Inset microscopic images represent the morphological view of a respective gel-like structure.

To further proceed towards understanding the effect on $E_{CB\text{-}CO}$, parallel experiments were performed on pure CB and CO. As similar to $E_{CB\text{-}CO}$, phase separation is observed in case of 2, 3 and 5 wt% of C (30) in CB, along with showing 'gel-like' network of long rods entrapping crystals of CB in between. As shown in figure S2(a), for sample of 2 wt% C (30) addition, the red line represents continuous network of C (30) crystals in which tiny granulitic crystals of CB at the surface of these rods and the space in between are entrapped. Hence, the microstructural view provides a resemblance towards an oleogel like structure.

Similar to $E_{CB\text{-}CO}$, the macroscopic view of glass bottles for samples of pure CO and its comparison with 1, 2, 3 and 5 wt% of C (25) and C (30) are shown in figure S2(b). As CO tends to crystallize after 24 h, the behavior of 'oleogel-like' property was observed after 1 h and 24 h. After comparison with pure CO, the samples with 2, 3 and 5 wt% of C (25) and all samples with C (30), after 1 h, demonstrate the opaque mixture compared to the transparent liquid part of CO. The 'oleogel' type structure can be confirmed by inverting the glass bottles of 3 and 5 wt% of C (25) and C (30) (figure S2(b)). The comparison with the microscopy images depicts that, after 1 h, the C (25) crystallizes (unspecified or vague morphology) and entraps the liquid oil. Whereas, after 24 h, the needle-like morphology from CO crystals appeared (figure S2(c)). Such specific behavior after 1 h could be because CO is in liquid state, while, a network of C (25) behaves as isotropic and hence partially polarized micrographs are detected. Therefore, the difference between liquid domains and C (25) crystals is hard to detect in case of samples with 3 and 5 wt% C (25) addition. However, in case of C (30) addition to CO, the network formed by C (30) crystals inhibits the long needle-like growth of CO crystals by restricting the phase space. Therefore, our observation depicts that small spherulitic crystals are formed instead of long needles due to the aggregation of needles. This suggests that as the length of C (30) is higher, the more robust connectivity of C (30) crystals is to be achieved and hence, entrapped CO can not be crystallized in the long needle-like structure due to C (30) crystal barrier. Thus, the micro and macroscopic observation provide a hint towards the formation of oleogel-like behavior.

Therefore, according to these initial observations, phase separation occurs at a higher percentage of C (25) and C (30) in all CB, CO, and $E_{CB\text{-}CO}$ mixtures. The possible reason for these phase separations at a higher percentage would be the center to center distance of one to another molecule of C (25) and C (30) decreases as the concentration increases. This eventually leads to fast segregation of 'like' molecules and thus the solidification of n-alkanes takes place earlier and separated from rest of liquid and solid fraction. In addition, n-alkanes likely provoke a "selective crystallization" of saturated fats. Hence, to avoid the effect of phase separation, in our further study, we have decided to characterize only the impact of 1 wt% of C (20), C (25) and C (30) on the crystallization of $E_{CB\text{-}CO}$, CB and CO in terms of the effect on thermal, morphological and mechanical properties and further understand the mechanism for variations in these properties.

3.2. Thermal behavior

3.2.1. Effect of n-alkanes on $E_{CB\text{-}CO}$

After keeping the samples for 24 h at 22 °C the thermal behavior of $E_{CB\text{-}CO}$ with n-alkanes was analyzed by using DSC. In case of the 1st melting process, no specific thermogram is observed; hence only crystallization and re-melting behavior are shown in Fig. 2 (a). Each color represents a different mixture of $E_{CB\text{-}CO}$ with n-alkanes, which are compared with the control sample (pure $E_{CB\text{-}CO}$). During crystallization, for 1 wt% of C (20) and C (25), the onset temperature, as well as the main exothermic peak, has shifted to a higher temperature (peak ~ 8 °C) as compared to pure $E_{CB\text{-}CO}$ (peak ~ 4 °C). Whereas in the case of 1 wt% of C (30), two exothermic peaks appeared, one at ~ 30 °C and followed by a second at ~ 10 °C. The exothermic peak at 30 °C represents the crystallization of C (30) compared to the DSC patterns of pure n-alkanes (Supplementary Figure S3). These two different exothermic peaks represent that a mixture of 1 wt% C (30) with $E_{CB\text{-}CO}$ displayed phase separation in solid-state. Moreover, these results also propose that high melting fractions (HMF) of eutectic mixtures (from CB or CO) interact or co-crystallize with n-alkanes and hence tend to crystallize at the higher temperature. After crystallization to −50 °C, the melting process was implemented to observe the variations in melting behavior after the addition of n-alkanes to the eutectic mixture. This result illustrates that for all the mixtures, the melting temperature is increased with respect to the eutectic mixture; however, no significant change is observed for three different alkyl chain lengths. These results confirm that addition of 1 wt% of C (20) and C (25) shows an increase in crystallization temperature with no indication of phase separation, whereas a phase separation occurred at 1 wt% of C (30) in solid state.

This result shows a significant change in the thermal behavior of $E_{CB\text{-}CO}$, but it is difficult to predict specific reasons behind it, hence, in further experiments, 1 wt% of n-alkanes were mixed with CB and CO and their analysis is explained in sections a and b below. These sets of experiments led us to understand the interactions of pure components with different chain length n-alkanes and thus the thermal behavioral changes.

3.2.2. Effect of n-alkanes on CB

The thermal behavior of CB with three different segments is shown in Fig. 2 (b). Each color represents a different blends with n-alkane (black, red and green) and their comparison with pure CB (blue line). After 24 h at 22 °C, DSC was performed for each different additives and their

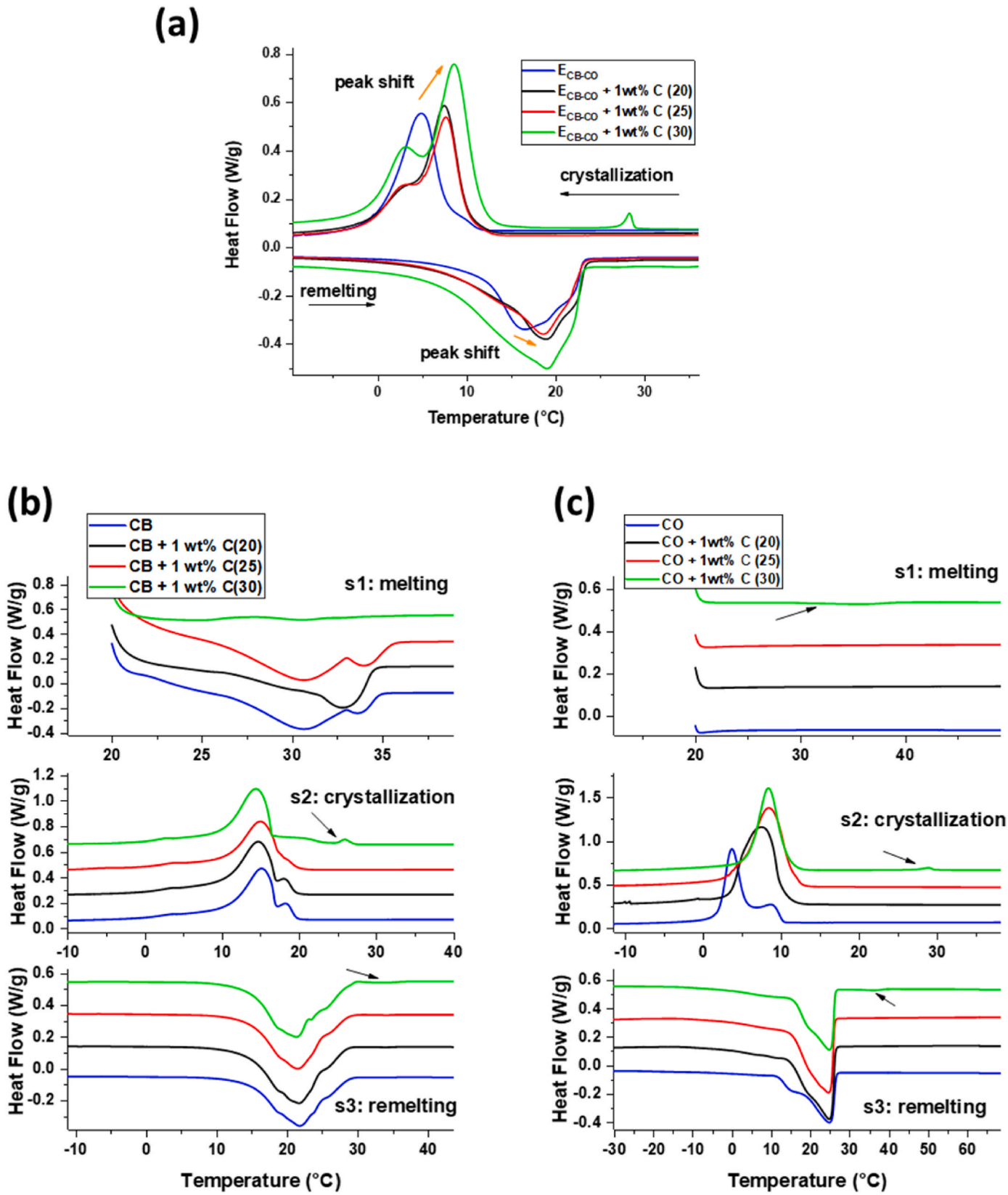

Fig. 2. (a) DSC thermogram of effect of n-alkanes on (a) crystallization and re-melting process of E_{CB-CO} (b) melting, crystallization and re-melting of CB and (c) CO. Their comparison with thermal property of E_{CB-CO}, pure CB and CO respectively. Orange arrow in (a) depicts the shift of exotherm and endotherm of E_{CB-CO} after addition of 1 wt% of n-alkanes to higher temperature. In figure (b) and (c) the exotherm and enotherm peak of C (30) crystal is indicated by black arrow. (For interpretation of the references to color in this figure legend, the reader is referred to the Web version of this article.)

melting segment was plotted as segment 1 (s1). In case of pure CB, two endothermic polymorphs, Form IV (30.85 °C) and Form V (33.6 °C) (Wille et al., 1966). After adding 1 wt% of C (20), one sharp peak is obtained at ~ 33 °C (Form V), along with a smeared out peak at lower temperatures than 33 °C. However, samples of 1 wt% of C (25) do not show any significant difference in the melting pattern compared to pure CB profile. While after the addition of 1 wt% C (30) a tiny melting peak is detected.

The next segment (Fig. 2 (b) s2) was designed to observe the effect of dynamic crystallization on the individual fat and their respective blends. A controlled cooling process was achieved in this segment that led to the formation of crystal forms that are different from those formed during the 24 h isothermal crystallization process. As explained in our previous study (Joshi et al., 2020), pure CB crystallized according to the composition of TAGs present in the CB. The co-crystallization of the high melting fraction (HMF), a medium melting fraction (MMF) and a low melting fraction (LMF) took place. For the addition of 1 wt% of C (20) and C (25), there is no specific change in peak temperature detected, whereas, for 1 wt% of C (30), two exothermic peaks appeared, one at ~ 26 °C and another at ~ 14 °C. By comparing this exotherm with pure CB and thermogram of pure n-alkane (supplementary Figure S3), the peak at 26 °C represents the C (30) crystals, whereas the peak at 14 °C detected is for CB crystals. Another observation is that HMF peak at 1 wt % C (25) and C (30) is diminishing as compared to pure CB, which can suggest that the HMF of CB interacted with C (25) and C (30); however, a similar phenomenon is not observed for 1 wt% C (20). After the crystallization process, the re-melting process is shown in Fig. 2 (b) s3. Unfortunately, after adding n-alkanes to CB, it does not show any specific change in melting temperature with respect to chain length. Thus, this result highlights that there is an effective change in the crystallization of CB after the addition of 1 wt% of C (20) during isothermal crystallization (segment 1) as compared to dynamic crystallization (segment 3). Moreover, a phase separation at solid state in case of 1 wt% addition of C (30) emerged, similar to a eutectic mixture (Fig. 2). On the other hand, no evidence of an increase in melting temperature with respect to the addition of n-alkanes is observed.

3.2.3. Effect of n-alkanes on CO

Fig. 2 (c) shows three segments of melting, crystallization and re-melting for 1 wt % of n-alkanes in CO with respect to pure CO. Each different color represents 1 wt% of C (20), C (25) and C (30) respectively. In case of CO, after 24 h, the crystals are formed; however, it is already in the molten form before starting the measurement due to the handling process hence no endothermic peak is detected except for 1 wt % C (30). The small endothermic peak is detected at ~36 °C. This peak represents the melting temperature of 1 wt% C (30). The next segment shows the crystallization of these blends with a rate of 2 K/min. For pure CO, two crystallization exotherms are detected, in which one is a sharp peak at a lower temperature (~2.5 °C) and the second overlapping shoulder peak at a higher temperature (~7.4 °C). After the addition of 1 wt% of C (20), the peak temperature is shifted to ~ 8 °C. Similarly, after adding 1 wt% C (25), the peak shifted more to the higher temperature, suggesting that higher carbon chain length enhances the crystallization in pure CO. However, in case of 1 wt% C (30), the peak temperature is not further shifted towards higher temperature, instead, another small exothermic peak is detected at ~ 28 °C. Altogether, this result proposes that the addition of long-chain hydrocarbon helped increase the crystallization temperature of CO along with phase separation. A similar effect is obtained during the crystallization process for $E_{CB\text{-}CO}$.

During the re-melting process, CO shows two peaks, one main peak at ~24 °C and another shoulder peak at ~14 °C, which reflects the melting of HMF and LMF. After the addition of 1 wt% of C (20) (black curve), the peak temperature is not changed; however, the shoulder peak at 14 °C disappeared. This endotherm is in accordance with the exotherm profile in Fig. 2 (c) s2 of the same blend as it tends to crystallize as a single peak. This suggests that adding n-alkane helped prevent the co-crystallization process in case of CO by providing the necessary surface "seed" to crystallize as a one crystal form. A similar effect of vanishing shoulder of melting peak is observed after the addition of 1 wt% of C (25) and C (30). Likewise, it has been found in a study that after addition of 1 wt% of low HLB sucrose esters to coconut oil resulted in minor changes in melting temperature with no influence on polymorphic occurrence (Chaleepa et al., 2010a). Thus, these results offer compelling evidence for our hypothesis that interaction of CO with derivatives of n-alkanes is more pronounced than CB; hence, the effect on the eutectic mixture is distinctly noticeable.

Our DSC experiments suggest that the crystallization and melting temperature of the eutectic mixture increase after adding all the derivatives of n-alkanes. Further analysis confirms that the interaction of CO with n-alkanes induces such behavior due to the attractive interaction of CO with n-alkanes. Although fast crystallization has been discussed, the question remains, which kinds of interactions takes place between CO and n-alkanes crystals for inducing the crystallization process. To put further steps towards understanding this phenomenon; the following hypothesis is necessary: The crystal structure of n-alkanes and their compatibility with the crystal structure of CB and CO results in a non-favorable and favorable interactions, respectively. However, before understanding these interactions, the mechanism for the formation of eutectic mixture needs to be understood.

The formation of stable nuclei requires total overcome a certain (free) energy barrier which is determined by the volume and surface energy balance. Our preliminary experiments shows that, the formation of nuclei and the crystallization of CO initiates from the edges of the vessels or microscope slides and progresses to the center.

A) Due to the structural difference between TAGs of CB (mono-unsaturated TAGs), the attachment of these TAGs to the short-chained saturated TAGs of CO increases the total free energy of the system. On the contrary, the detachment or deagglomeration of CB crystal from CO crystals reduces the free energy to the states of higher preference.
B) Another point appears from the supercooling as the crystallization temperature is 22 °C (CT), close to CB and CO's melting temperatures. The CB and CO crystals have ample time to arrange the best possible lamella having stable 3D nuclei with the least amount of free energy and surface energy.

Therefore, point A and B illustrates that the demixing of CB and CO could take place for all the CB-CO blends except for the crystals formed at eutectic mixture composition.

To further elaborate this hypothesis with respect to the addition of n-alkanes in $E_{CB\text{-}CO}$, the concept of a) epitaxial growth b) heterogeneous nucleation can be taken into account. Already formed crystals of n-alkanes act as a seed for the initiation of CO crystallization. The strong van der Waals attractive forces between template molecule and CO depend on the crystal structure conformation. According to the previous studies, the crystal formation of n-alkanes differs with respect to the chain length and evenness (in the number of carbon atoms), pure n-alkanes crystallize in monoclinic (even carbon $n > 26$), tri clinic (even carbon $n < 26$) or depending on temperature, odd n-alkanes crystallize in an orthorhombic or pseudo-hexagonal structure (Sangwal, 2007). Here, C (20) and C (25) derivatives are even and odd chain length having less carbon atom than 26 respectively hence, tend to crystallize in triclinic and in an orthorhombic or pseudo-hexagonal for C (25) respectively. Similarly, the polymorphic formation of CO and CB tends to acquire typically hexagonal, orthorhombic, and triclinic crystal structures depending on process conditions (Sato, 2018). Hence, when the triclinic crystal structure of C (20) is mixed with $E_{CB\text{-}CO}$ and in CO individually, the crystallization temperature increases due to the epitaxial growth mechanism (Ishibashi et al., 2017). Beacuse of the similarity in crystal orientation and chain length of CO and C (20) & C (25), the lamellar distance and subcell packing become analogous; which ultimately

results into attractive interactions (van der Waals forces) between molecules. Furthermore, due to the similar subcell packing, the interfacial energy becomes less and thus the activation energy for nucleation of CO decreases. Whereas in case of the addition of C (30), the monoclinic crystal structure tends to occur, which exhibits different behavior with respect to the crystal structure of TAGs from CO. Due to these differences in the crystal structure, the phase separation between CO and C (30) crystals occurs. Although there appears a phase separation in polymorphic form these crystals from C (30) act as nucleation sites (heterogeneous nucleation process) for further crystallization and hence increase in crystallization temperature is observed. In contrast to the effect on CO crystallization, the effects on CB crystallization is hardly noticeable. The reason could be that even though the similarities in crystal structure from C (20) and C (25) to CB crystals, the lamellar spacings increased due to the presence of a double bond in the oleic acid. Thus, only HMF from CB, which contains mainly saturated TAGs show van der Waals attractive forces with triclinic or orthorhombic crystal structure. Therefore, the disappearance of shoulder peak from Fig. 2 (b) s2 is observed. Whereas, in case of C (30) addition again due to dissimilarities between crystal orientation (monoclinic of C (30) and CB crystals (form I, hexagonal) and lamella spacings (due to double bond), the phase separation occurs.

3.3. Ternary plot: liquidus temperature projections

It is useful to construct a ternary diagram with liquidus melting temperature projections to understand the possible forecast of effect of chain length of n-alkanes on the melting temperature profile of the ternary system. To elaborate this in more detail, the ternary temperature profile is plotted by considering the melting temperatures (s3: re-melting segment in Fig. 2) of mixtures: one ternary mixture of CB, CO and n-alkanes ($E_{CB\text{-}CO}$ + 1 wt% n-alkanes), 2 binary mixtures of CB and CO with n-alkanes (CB and CO + 1 wt% n-alkanes) and the melting temperatures of liquidus line of 12 binary mixtures of CB/CO blends from our previous study (Joshi et al., 2020) (shown the graph in Fig. 3 (d)) and the melting temperature of individual components. Fig. 3 (a), (b) and (c) represent the ternary temperature profile diagram with the specific indications of contours having least temperature (blue region) to highest possible temperature (red region) for further mixtures of ternary components of C (20), C (25) and C (30) addition to CB and CO

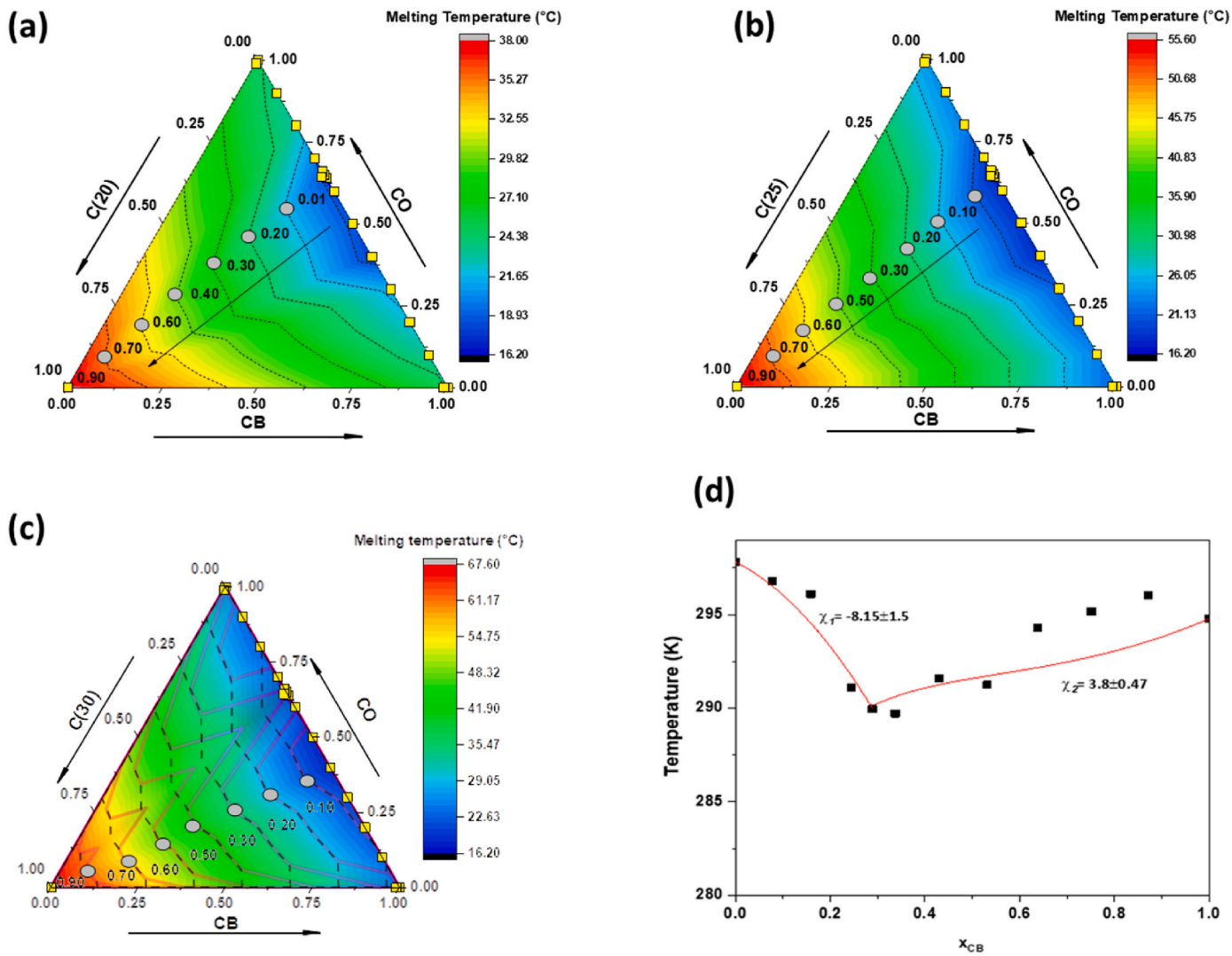

Fig. 3. Ternary plot with melting temperature projections with respect to the concentrations (a) C (20)-CB-CO (b) C (25)-CB-CO (c) C (30)-CB-CO ternary plot. The sidebar represents the change in temperature with respect to the color. Yellow square symbols indicate measured data points and filled gray circles on boundary lines represent the concentration of n-alkanes on that position to understand the effect of chain length concentration on melting temperature of ternary mixtures. In case of C (30) ternary plot, the superimposition of predication n from two different melting points from DSC results is shown. Solid line predictions belong to C (30) melting points and a dashed line indicates the main peak temperature (CB, CO and $E_{CB\text{-}CO}$). (d) The liquidus line for CB/CO blends is plotted based on DSC results from our previous study (Joshi et al., 2020). (For interpretation of the references to color in this figure legend, the reader is referred to the Web version of this article.)

respectively. The three sides of triangles represent the weight fraction of the individual components, as indicated by the increasing concentration arrow. Different color profiles are separated by boundary lines displayed with dashed black lines. The respective temperature limits for each boundary line is shown on the vertical bar next to the ternary diagram. The filled gray circle on each boundary line belongs to the point with a specific concentration of ternary mixture and only the fractions of respective n-alkanes in the mixture is shown as black text. For instance, in the ternary mixture for 1st point in Fig. 3 (a) indicates (weight fraction of C (20)) $X_{C(20)} = 0.01$, then the 2nd point indicates $X_{C(20)} = 0.15$, and so on. The data points from our experiments are shown as yellow squares. Based on these data points, the possible forecast of the ternary temperature state diagram for all concentrations is possible. In case of C (30) ternary diagram (Fig. 3 (c)), the superimposition of two plots are shown. As DSC profiles of C (30) addition to $E_{CB\text{-}CO}$, pure CB and CO show two melting peaks, the solid line represents the possible forecast obtained by considering the melting temperature of C (30). In all three diagrams, dark blue indicates the least melting temperature for ternary blends of CB, CO and n-alkanes. The ternary mixture of C (20) and CB-CO indicates the formation of a eutectic phase with a range from X_{CO} = ~0.37 to 0.70 with up to $X_{C(20)}$ = ~0.05. Moreover, the light blue contour in case of C (20) addition also shows the eutectic phase with increased concentration range of CO from ~0.22 to 0.75 with up to ~0.15 of C (20). For further concentrations of C (20), the green region estimates the elevation in melting temperature of the ternary mixture. Similarly, a higher concentration of CO and/or CB with less amount of C (20) will increase the melting temperature of the ternary mixture. As the concentration of C (20) further increases, the melting temperature will increase as expected.

On the other hand, in case of C (25), the ternary eutectic forms with the range from ~0.37 to 0.75 of CO and up to ~0.08 of C (25). Although the prediction represents the eutectic mixture with such a high percentage of C (25), the predictions contradict the DSC and initial microscopy result as it tends to phase separate above 2 wt% for C (25). For further concentration of C (25), the melting temperature of ternary phase is increasing with the effect of phase separation. In case of ternary plot for C (30), the dashed line and solid line plot suggest that the ternary eutectic forms with the range from ~0.37 to 0.75 of CO and ~0.37 to 0.55 of CO up to the ~0.10 of C (30) respectively. For further concentrations, the dashed line plot represents similar predictions as C (25) ternary plot, whereas solid line estimates imply that in the range of ~0.55–0.75 of CO, the least melting temperature has been predicted as compared to the other compositions on that boundary line.

From these ternary plots, a similar trend for C (25) and C (30) addition is predicted. This is due to 1) the presence of higher carbon chain length as compared to the one in CB and CO, and 2) there is a large difference in melting temperature of CB & CO and C (25) & C (30). While on the contratry, the eutectic mixture formation with a higher concentration of C (20) is possible because of fewer differences in melting temperature and with chain length. Hence, irrespective of chain length with 1 wt% of n-alkanes addition to $E_{CB\text{-}CO}$ does not show any significant change in melting temperature but with higher percentage may increase the melting temperature up to ~22 °C with a consequence of phase separation in case of C (25) and C (30).

3.4. Crystal morphology

The crystal morphology of n-alkanes addition to $E_{CB\text{-}CO}$ blends was captured by PLM. Fig. 4 (a) shows the morphology of 1 wt% of C (20), C (25) and C (30) to $E_{CB\text{-}CO}$ after 24 h at 22 °C and after heating this sample to 90 °C and cooled down to 10 °C with 2 K/min rate. The pictures captured after 24 h at 22 °C display the crystal formation after the isothermal crystallization process. Hence one can understand the morphology of crystals, which are melted during the DSC melting segment. Although the crystallinity of eutectic mixture and n-alkanes are visible in microscopy, the DSC could not measure endotherm for these tiny crystals; hence, this result is not shown in Fig. 2. According to images, after the addition of 1 wt% of C (20), C (25), and C (30), aggregation of small needlelike morphology is observed. Moreover, the crystallinity is increased as compared to $E_{CB\text{-}CO}$, which is studied in our previous work (Joshi et al., 2020). While in the case of dynamic crystallization, the granular structure is formed in all blends. Similar to DSC, a morphological study is also performed on CB and CO to understand the effect of carbon chain length on morphology. In Fig. 4 (b), the crystal morphology of 1 wt% of C (20), C (25) and C (30) to CB after 24 h at 22 °C and after heating this sample to 90 °C and cooled down to 10 °C with 2 K/min rate is shown respectively. These images, after 24 h detected spherulitic morphology for 1 wt% of C (20), whereas granulated structures are observed for 1 wt% of C (25). While in case of 1 wt% of C (30), randomly shaped aggregates of small crystallites are formed. After heating at 90 °C and cooling down to 10 °C, the crystal morphology formation shows the crystallization process from DSC (Fig. 2 (b) s2). At 10 °C, in all blends, small granulites are observed, which is similar to morphological behavior observed in pure CB (Joshi et al., 2020).

Similar experiments were performed on CO; Fig. 4 (c) shows the images captured after 24 h at 22 °C and crystal morphology after dynamic crystallization at 10 °C. Needle-like morphology is observed after 24 h for the addition of 1 wt% of C (20) and C (25), whereas, for 1 wt% of C (20) and C (25), small spherulites from an aggregation of needle-shaped crystals are formed and grew until their surface-merge. Similar phenomena occurred in case of 1 wt% of C (30) for crystal growth; however, there is a hint of another crystal form (rod-like) marked with a red arrow in the figure. According to crystal morphology from pure n-alkanes (Supplementary Figure S4), this rod-like morphology represents the crystals of C (30). Therefore, these two different forms of crystal structure represent the phase separation, which agrees with DSC results. Accordingly, the result demonstrates that, although the addition of 1 wt % of n-alkanes in $E_{CB\text{-}CO}$ does not influence the crystal morphology a lot, the increase in crystallites after 24 h leads to a hypothesis of increasing solid fat content. Similar results were observed in case of 1 wt% of sucrose esters in CO showed no effect on polymorphism and morphology but crystallization kinetics (Chaleepa et al., 2010b). Hence, to verify this theory, SFC was calculated based on ^{1}H solid-state NMR experiments.

3.5. Effect of n-alkanes on crystallization kinetics

To understand the effect of n-alkanes addition to $E_{CB\text{-}CO}$ and CB, CO, in terms of solid fat content (SFC (%)), isothermal crystallization kinetics is studied. Fig. 5 (a), (b) and (c) show the graph between the relation of SFC after addition of C (20), C (25), and C (30) on pure $E_{CB\text{-}CO}$ and CB, CO respectively. The blue graph represents the control samples for three different mixtures. The insets show the magnification at early times of the crystallization kinetics from the original graph. According to Fig. 5 (a), after adding three different n-alkanes to $E_{CB\text{-}CO}$, the SFC value increases to ~ 7% from ~5% (control sample). No significant influence of carbon chain length on final SFC is detected. Moreover, magnifying view reveals that for 1 wt% of C (20) and C (25) addition, the crystal growth occurs similar to $E_{CB\text{-}CO}$, while in case of 1 wt% of C (30), the crystal growth is faster than the other blends. In order to understand the effect of adding n-alkanes in $E_{CB\text{-}CO}$, similar experiments were carried out on CB and CO. According to Fig. 5 (b), the SFC profile is influenced with respect to chain length as well as a pure CB profile. The SFC value after 24 h for all the blends also shows a similar value (~70%). This result suggests that the SFC value of CB is not affected by a small amount of n-alkanes and therefore there is no specific change in thermal behavior observed.

In contrast with the results for CB, the addition of n-alkanes to CO (Fig. 5 (c)) shows a significant change in crystallization kinetics; however, the SFC value after 24 h hardly differs (~22%). According to the magnifying view, the crystal growth for 1 wt% of C (20) and C (25) is delayed as compared to pure CO, whereas, for 1 wt% of C (30) the crystal

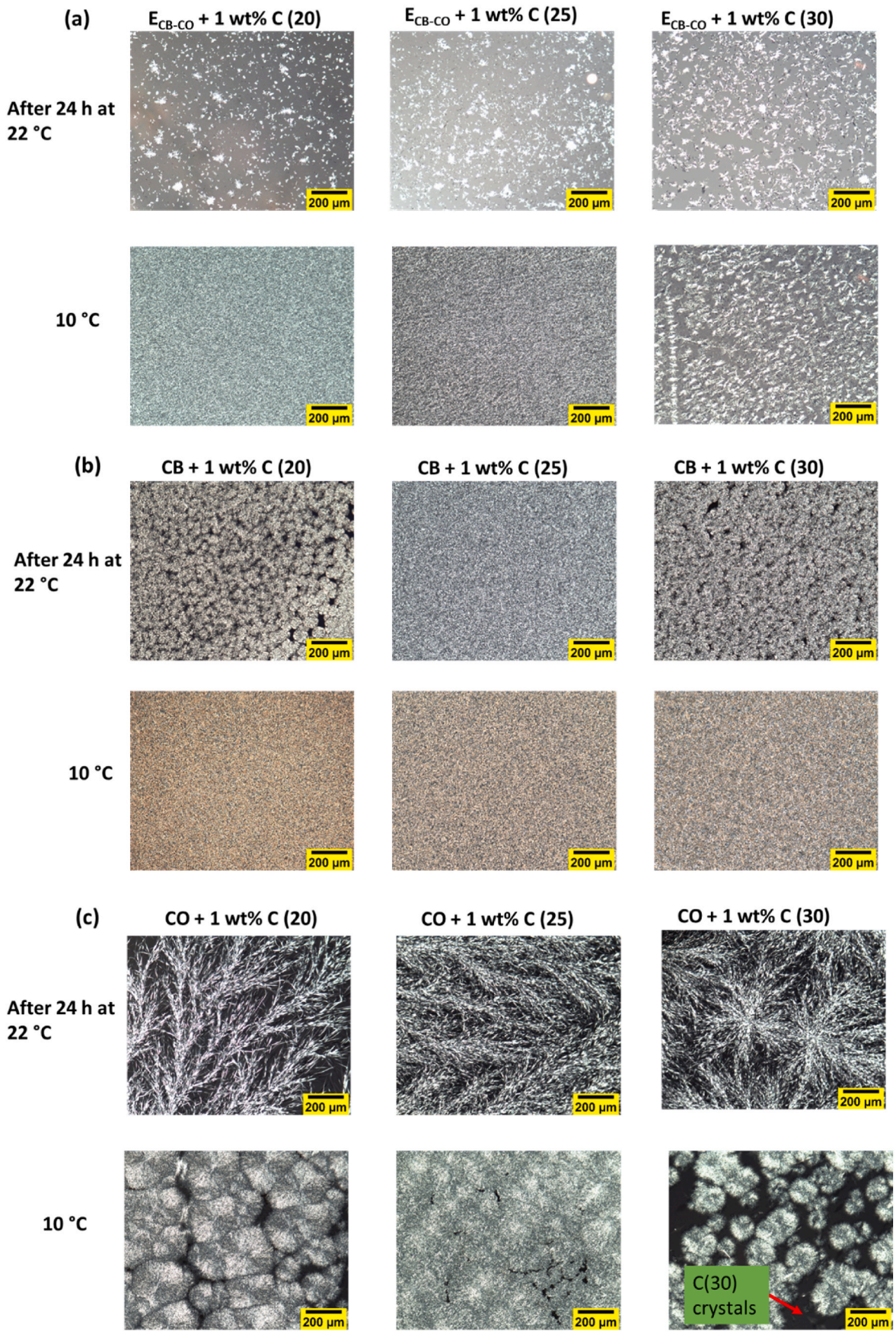

Fig. 4. Microscopic representation of changes in morphology with respect to the addition of 1 wt% of C (20), C (25) and C (30) in (a) E_{CB-CO} (b) CB and (c) CO after 24 h at 22 °C (showing results of isothermal crystallization) and at 10 °C after dynamic crystallization process. The scale bar represents 200 µm.

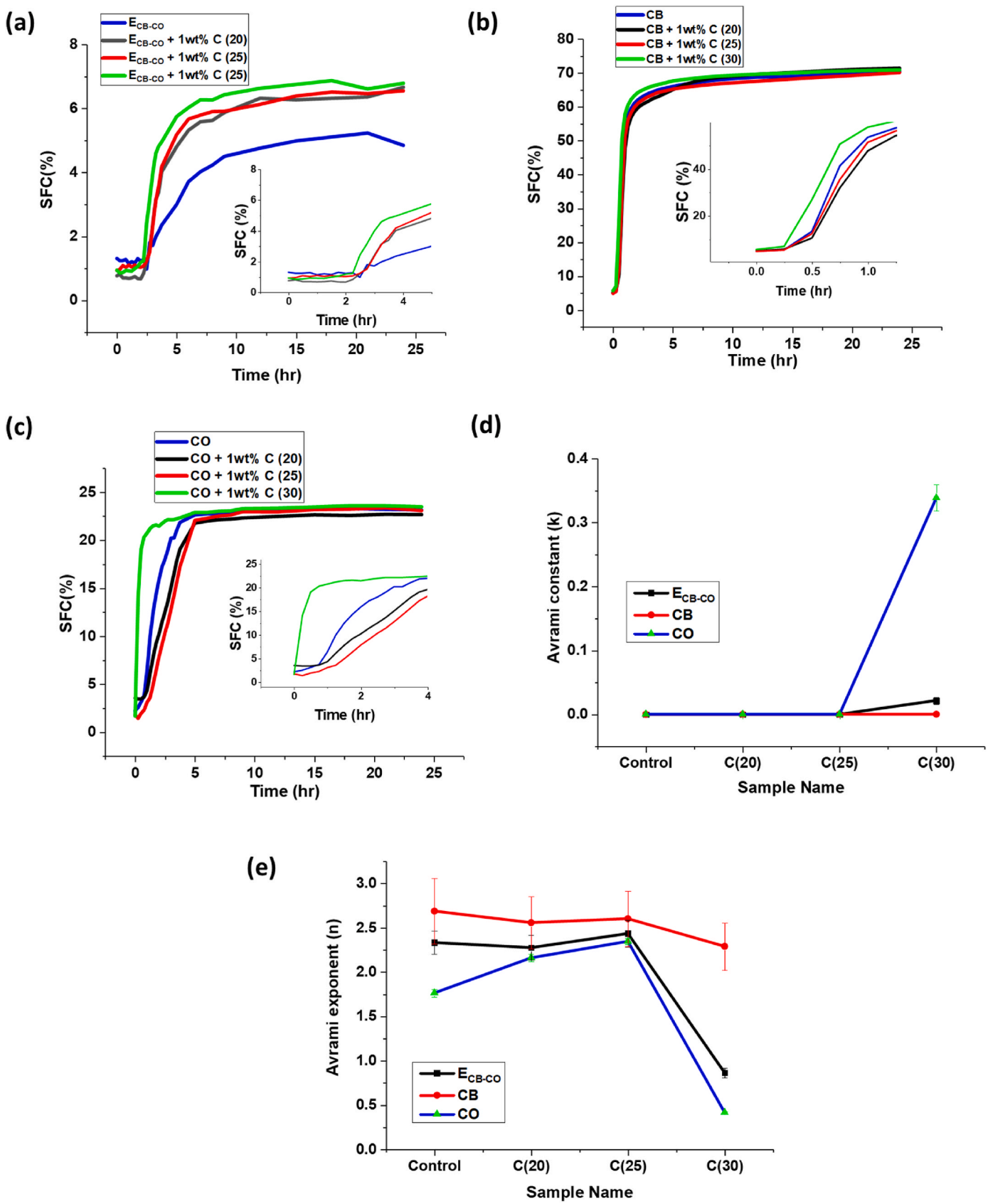

Fig. 5. Effect on solid fat content (SFC) profile for addition of 1 wt% of C (20), C (25) and C (30) in (a) $E_{CB\text{-}CO}$, (b) CB and (c) CO respectively. The inset graph represents the magnifying view of start of crystallization process. The SFC profile is determined at 22 °C for 24 h timeline. (d) And (e) denotes Avrami constant (k) and exponent (n) change after 1 wt% of n-alkanes. Control represents pure $E_{CB\text{-}CO}$, CB and CO.

growth is promoted. A similar observation has been shown in case of the studies of adding diacylglycerol as a minor component to anhydrous milk fat, resulting the delay in the onset of crystallization at low degrees of supercooling (Wright et al., 2000). The possible reason for the prohibition of nucleation with C (20) and C (25) is to promote dense crystal lamella, which would lead to thermodynamically stable nuclei due to similarities in molecular structures of CO and C (20) & C (25). Therefore, in the case of DSC results the crystallization temperature increased. Altogether, the crystallization kinetics profile explains why there is a change in thermal behavior after adding n-alkanes to pure CO.

Similar to DSC results, SFC profiles for all the samples depict that, in the eutectic mixture; the effect is prominent after adding n-alkanes. This effect would also be due to distinct interaction between CO with n-alkanes as compared to CB. For more understanding of crystallization kinetics, all the profiles were fitted with the Avrami equation (Supplementary Figure S5). After fitting this equation, k (Avrami constant) and n (exponent) were acquired (a fitting example is shown in the Supplementary Figure S5). In Fig. 5 (d), the relation of k with respect to the chain length of n-alkanes is shown. Avrami constant (k) for 1 wt% of C (20) and C (25) obtained similar value as $E_{CB\text{-}CO}$, which reflects that no specific variation in nucleation and crystal growth, however, the sharply increased value for 1 wt% of C (30) represents an increase in crystallization rate due to seed crystals of C (30). Similar behavior is obtained for 1 wt% of n-alkanes in CO. A sharp increase in k value implies the phase separation due to the addition of C (30). Our results are in agreement with the study of addition of different amounts of candelilla wax (CLW) and rice bran wax (RW) in palm kernel stearin (PKS-85). The SFC content at 20 °C and 4 °C after 24 h have not significantly changed; however, it exhibited a higher value of k at 20 °C for the addition of CLW, implying promoting crystallization of PKS-85 (Liu et al., 2019).

Further, In case of CB blends, no specific effect on k value was observed after the addition of 1 wt% of C (20) and C (25) as compared to pure CB because of alike SFC profile as shown in Fig. 5 (b) (magnifying view). The reason for such behavior could be that a small amount of n-alkanes (specifically C (20) and C (25)) acted as a part of CB system and hence no specific change. Whereas, after adding 1 wt% C (30) to CB, the crystallization process is promoted as per magnifying view, but (k) value is hardly varied.

The Avrami exponent, *n*, originally meant to reflect the crystal growth geometry, provides evidence about nucleation and growth mechanism (Avrami, 1939, 1941). The phenomenological Avrami equation addresses the crystal growth as a combination of the function of the time dependence of nucleation and the number of dimensions in which growth occurs. Nucleation is either instantaneous, with all nuclei appearing at once, or sporadic, with the number of nuclei increasing linearly with time. Crystal growth could be either spherical, plate-like, or needlelike in three, two, or one dimension, respectively. Ideally, the exponent value is an integer; however, in most experiments, fractional values are observed due to the simultaneous development of more than one type of crystal. In this study, fractional values are obtained after fitting the equation, explains either the reason mentioned above or formation of similar crystals from different types of nuclei (Marangoni et al., 2012). Fig. 5 (e) shows the effect on exponent *n* with respect to chain length for $E_{CB\text{-}CO}$, CB and CO. Addition of 1 wt% of C (20) and C (25), to $E_{CB\text{-}CO}$, represent similar value as a control for avrami exponent, while a decrease in ($n\sim 1$) for 1 wt% of C (30) is obtained. This result shows that formation of needle-like growth from sporadic nuclei in case of pure $E_{CB\text{-}CO}$ and addition of C (20) and C (25). This could be due to the low degrees of supercooling, resulting in higher free energy and lower nucleation rate, thus leading towards sporadic nucleus formation (Marangoni et al., 2012). While for 1 wt% of C (30), addition leads to a lower value, which can be due to the presence of rod-like structure of C (30) crystals. However, the formation of spherulitic structure cannot be detected with these sets of fittings. For CB blends, the (*n*) value is in the range of ~2.7 to ~ 2.5 from pure CB to 1 wt% of C (30) addition. This result suggests the formation of spherulitic crystals from instantaneous nucleation due to high degrees of supercooling, resulting in lower free energy and a higher rate of nucleation, thus forming a large number of nuclei (Marangoni et al., 2012). In contrast to CB blends, (n) value increase until C (25) and decrease for 1 wt% C (30) after addition to CO. These values indicate, rod/needle/fiberlike crystal growth from either instantaneous or sporadic nucleation (Marangoni et al., 2012). According to our microscopy images (Fig. 4 (c) _after 24 h at 22 °C), all three blends represent the needle-like growth. However, the possibility of formation of sporadic nuclei after addition of 1 wt% C (20) and C (25) results into increase in exponent value and for 1 wt% of C (30), the high degrees of supercooling between C (30) crystals and crystallization temperature results into instantaneous nucleation of rod-like structure from C (30) crystals.

Thus, according to the Avrami fitting results and microscopy images, the epitaxial growth mechanism in case of 1 wt% addition of C (20) and C (25) may occur, whereas heterogeneous nucleation is found in case of 1 wt% C (30) addition. These results support the hypothesis predicted according to the DSC results in section 3.2. Similarly, a study on difference between epitaxial and heterogeneous nucleation is carried out on crystallization of palm mid fraction on two template molecules: sorbitan tripalmitate and sorbitan tribehenate. Due to similar molecular structure, chain length of sorbitan tripalmitate and palm mid fraction, epitaxial growth mechanism is responsible for crystal growth, whereas, the difference in chain length, heterogeneous nucleation takes place with respect to sorbitan tribehenate (Ishibashi et al., 2017).

3.6. Effect of n-alkanes on mechanical properties

Rheological properties of pure fat and fat/oil blends are widely explored for understanding the fundamental relation between microscopic to macroscopic levels. Our study focused on studying the effect of n-alkanes addition to $E_{CB\text{-}CO}$ in terms of rheological properties and its comparison with pure $E_{CB\text{-}CO}$. To understand the variation in mixtures' rheological properties during temperature and time sweeps, only the storage modulus is considered for better visualization and interpretation. Fig. 6 (a), (c), and (e) represent the crystallization kinetics under the rheometer in terms of temperature and time sweeps. The brown graph denotes the temperature change with respect to time. While Fig. 6 (b), (d) and (f) display the amplitude sweep profile after 2 h 30 min of the crystallization process. Each different color indicates a different mixture. The result suggests that in case of 1 wt% of n-alkanes addition to $E_{CB\text{-}CO}$, the storage modulus increases with respect to carbon chain length.

Additionally, the storage modulus compared to the pure eutectic mixture is also increased. The crystallization temperature (CT) (step when storage modulus increases or leaps) is detected as 22 °C for pure eutectic as well as for mixture with 1 wt% of C (20). Whereas CT increases to ~27 °C and ~30 °C for mixture with 1 wt% of C (25) and C (30) respectively. In case of a mixture with 1 wt% of C (30), stepwise crystallization is observed due to phase separation between C (30) crystals and the rest of the CB-CO mixture. This result is in line with the SFC profile from the NMR experiment in Fig. 5 (a). Similar to previous experiments, rheological properties were also further studied for pure CB and CO. Fig. 6 (d) shows that adding 1 wt% of C (20) and C (25) in CB does not significantly change CT. The mixtures show similar behavior of stepwise crystallization as pure CB except for C (30), which indicates a small step just before reaching the first plateau region. The small step represents the crystallization of C (30) crystals and another step suggests that either a polymorphic transition or co-crystallization of mixed crystals.

Moreover, the addition of n-alkanes to CB leads to a decrease in storage modulus. Due to enhanced interactions of HMF from CB with n-alkanes, the rest of the mixture remains in the liquid state at this particular timeline, resulting in a higher fraction of mobile phase entrapped in a crystal network. Therefore, the reduced storage modulus is observed as compared to pure CB. Altogether, the rheological profile

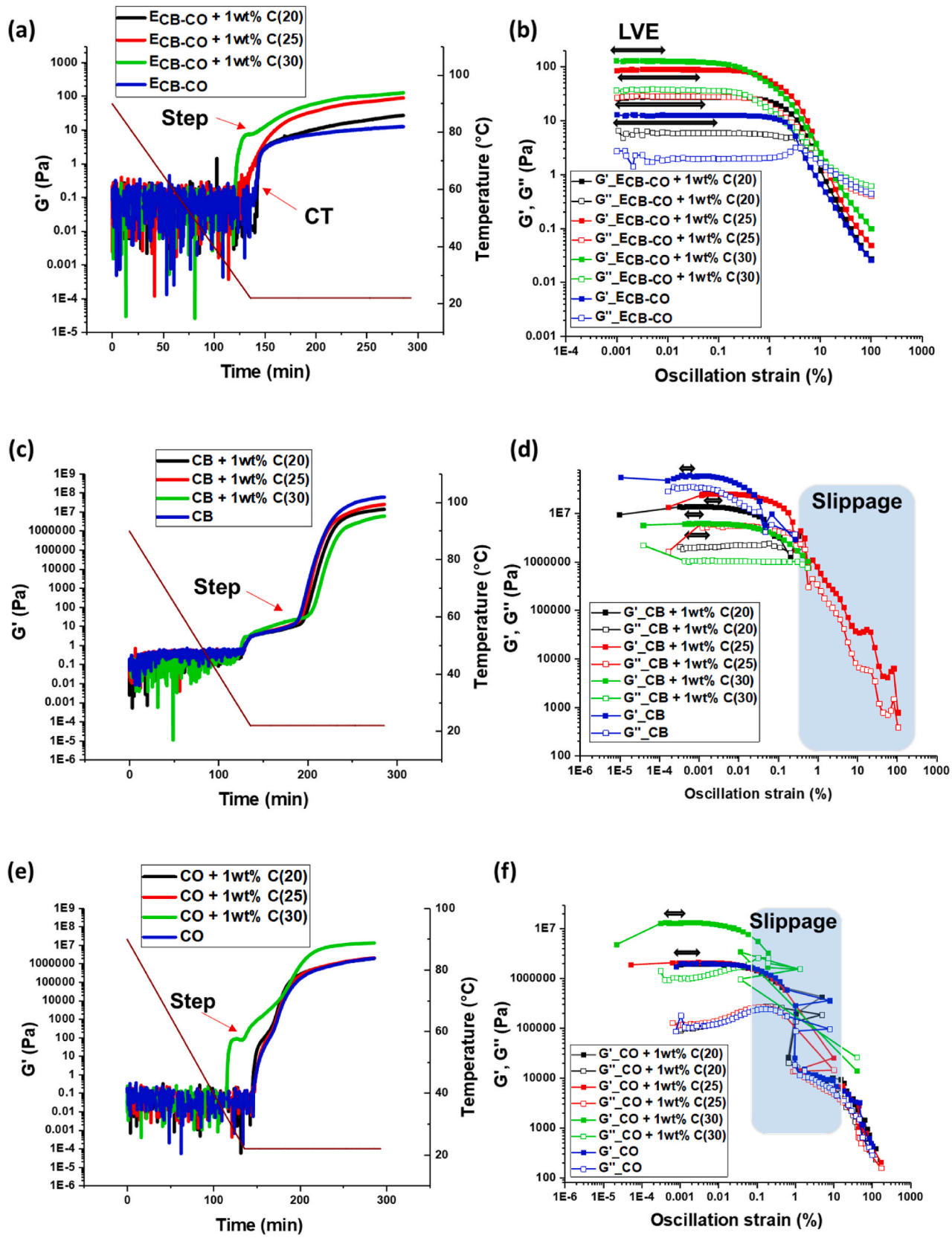

Fig. 6. Effect on rheological properties after addition of n-alkanes to $E_{CB\text{-}CO}$. (a), (c) and (e) represent temperature and time sweep plotted against time in minutes and brown graph profile is the temperature vs. time which provides precise temperature detection with respect to rheological properties for $E_{CB\text{-}CO}$, CB and CO, respectively. 'CT' represents the crystallization temperature position in each case where G' crosses over G''. (b), (d) and (f) represent the amplitude sweep profile for the same sequence. The slippage occurs in case of CB and CO samples due to high rigidity to jamming of needle-like morphology at higher strain values respectively. (For interpretation of the references to color in this figure legend, the reader is referred to the Web version of this article.)

for CB displays similar behavior as previous experiments from DSC and SFC profiles.

On the contrary to the effect on CB, adding n-alkanes displays differences in the rheological properties of CO. In case of 1 wt% of C (20) and C (25) with CO, the storage modulus value after 2 h 30 min is distinctly unchanged with respect to the pure eutectic mixture, whereas, for a mixture with 1 wt% of C (30), the storage modulus value increases significantly. Furthermore, the behavior is similar to a mixture of 1 wt% of C (30) with $E_{CB\text{-}CO}$: CT increases to ~35 °C along with stepwise crystallization, indicating phase separation. Thus, the result from crystallization kinetics under the quiescent condition (NMR result) and constant oscillation demonstrate similar findings. This observation shows that there is a stronger interaction of CO, (which is a mixture of short-chained saturated TAGs) and n-alkanes.

Further, the experiments continued with the amplitude sweep study to understand crystal networks' viscoelastic and structural properties. The strain amplitude sweep was performed for the range of strain from 0.001% to 100%. Closed symbols represent storage modulus (G') and open symbols as loss modulus (G''). These graphs are differentiated into linear and non-linear viscoelastic regimes represented as LVE and NLVE. According to Fig. 6 (b), G' is higher than G'', which points that sample behaves as 'elastic solid' for all the blends under small deformations. Moreover, the LVE range has decreased after adding 1 wt% n-alkanes to $E_{CB\text{-}CO}$ due to an increase in modulus (solidity). Whereas, in case of CB, the LVE range has increased after adding 1 wt% of n-alkanes compared to pure CB. Correspondingly in case of CO mixtures, 1 wt% of C (20) and C (25) display a similar LVE range as pure CO, while, decreased LVE range is observed after adding 1 wt% of C (30) due to higher modulus value.

Altogether, most of the fundamental work on fat crystals is performed in LVE range as it focuses on interaction forces establishing the connectivity of the crystal network. In the LVE range, the interparticle network, or in our case, the crystal aggregate network is held together by van der Waals's attractive and Born's repulsive forces (Kamphuis and Jongschaap, 1985). These forces can also be denoted as the bonds between the particle-particle clusters. Therefore, with a small amplitude, the stretching of these bonds between particles is small enough to leave the bond intact. Hence, any specific changes during a small amplitude could not be observed.

The breaking of a crystal network depends strongly on the type of morphology formed during the crystallization as the inter-particle bond stretching differs according to the geometry of crystals (Joshi et al., 2018). Therefore, all these different blends show a unique breaking behavior of the crystal network as each blend has a variety of (mixtures of needles and spherulitic) morphology under crystallization. In our study, typically three types of network breaking were observed: 1) In $E_{CB\text{-}CO}$ blends with n-alkanes only a small number of crystals are formed that are not interconnected. Hence, in this particular blend, the breaking is likely to refer to the dissolving of the small crystals back to a liquid and small fractures in individual crystals. 2) For CO and CB, the slippage at large deformations is observed and hence clear NLVE region does not occur. 3) In case of pure CO and blends with 1 wt% of n-alkanes, the slippage occurs from 1 to 10% of strain. To understand this in more depth, in situ rheo-microscopy was performed. This direct observation shows that as the amplitude increases, small branches of needles detach from the mother branch of the tree-like structures and these small needles further promote slippage. They are caged between the mother branches, and hence for higher amplitude, proper values cannot be detected. However, after breaking off small needles, the mobility of the upper geometry becomes smooth again and hence the measurement accurately took place.

The amplitude sweep for the blends with CB and 1 wt% of n-alkanes (Fig. 6 (d)) shows that the LVE range increases due to the presence of a higher amount of mobile phase entrapped in solid crystal network. Moreover, artifacts could also occur due to slippage (which is indicated as a blue surface). To understand the amplitude sweep profile profoundly, in situ microscopy with rheology was implemented. For the sake of understanding, only until 30 min, the crystallization was performed (as the increase in modulus (solidity) could destroy the glass plate geometry used instead of steel plate) for CB samples. This paper shows the result for only a blend with 1 wt% of C (25). The videos were captured from the upper plate towards the lower plate (see Supplementary V1). Hence, from in situ microscopy, we could show the movement of the 3D fat crystal network flowing according to the defined oscillatory force from crystals attached to upper geometry towards the lower glass plate. These videos were taken at the edge of geometry instead of center as the amplitude is higher at the edge thus the movement was easy to capture. Images extracted from these videos are shown in Fig. 7. At the beginning of each amplitude sweep, the crystals at the upper plate region (UPR) were captured, where no specific crystal morphology is observed. As the deformation increase, the middle region (MR) of 3D crystal network is visible, where needle-like random aggregative structure is observed.

Supplementary video related to this article can be found at https://doi.org/10.1016/j.crfs.2021.10.010

Further increase of amplitude leads to a decrease in G', which is indicated by an image at the lower plate region (LPR). In this image, the orange circles indicate the connection between spherical crystals due to an aggregation of needles. So it can be predicted that after a 10% increase in the amplitude, these spherical crystals leave their position from the networks and slide with each other. Thus, at the highest amplitude, the crystal network breaks down into individual crystals.

4. Summary

The results in this study indicate that the crystallization and melting temperature of a eutectic mixture $E_{CB\text{-}CO}$ increase after adding n-alkanes. Together with thermal properties, the solid fat content (SFC) and storage modulus (G') also increase compared to $E_{CB\text{-}CO}$. This behavior is the strong van der Waals attractive interaction of CO with n-alkanes, which leads to the promotion of the crystallization process in the blends. Based on current results, the possible schematic for interaction between $E_{CB\text{-}CO}$ and n-alkanes is shown in Fig. 8. Fig. 8 (a) demonstrates the terminology of the structure of n-alkanes along with pure CO and CB at solid-state. As CO and CB are mixtures of a large number of TAGs, the structure in Fig. 8 (a) displays the saturated (medium-chain (C (12:0)) and mono-unsaturated (C (18:1)) TAG, which are the main constituents of CO and CB respectively. Fig. 8 (b) shows the possible interactions occurring at the solid-state of ternary blends. According to the present results and previous studies on crystallization modifiers to lipid systems, the interaction of "seed" or "substrate" or "template" to the remaining part of lipid is strongly dependent on the chain length, molecular size, and saturation degree. Due to spatial arrangements of molecules, the ones having similar size and shape attract each other and may results into strong and dense crystal packing, hence leading to better physicochemical properties. At the same time, these modifiers at lower concentrations act as "template" to induce crystallization without affecting crystal morphology. This speculation was indeed confirmed with DSC, NMR, and PLM measurements, respectively. In this study, C (20), and C (25) acted as a seed to induce epitaxial crystalline growth, whereas C (30) encourages heterogeneous nucleation in a eutectic mixture. CO tends to crystallize from borders to the center of the system; hence, the addition of such templates or seeds to a eutectic mixture undeniably helped to crystallize faster and constitutes surfaces for aggregation of other TAGs from CO and CB. However, as C (30) length is much higher than CO and defects due to kink of CB, phase separation tends to occur. In case of C (20) addition, the possible strong interaction occurs between the alkyl chain of saturated TAGs from CO to the n-alkane. This lateral interaction of the alkyl chain results in closely packed arrangements and hence the better physicochemical properties of eutectic mixture obtains. There is a possibility that one molecule of C (20) interacts with the two alkyl chains of TAGs from CO as shown in Fig. 8 (b). The bilayer or

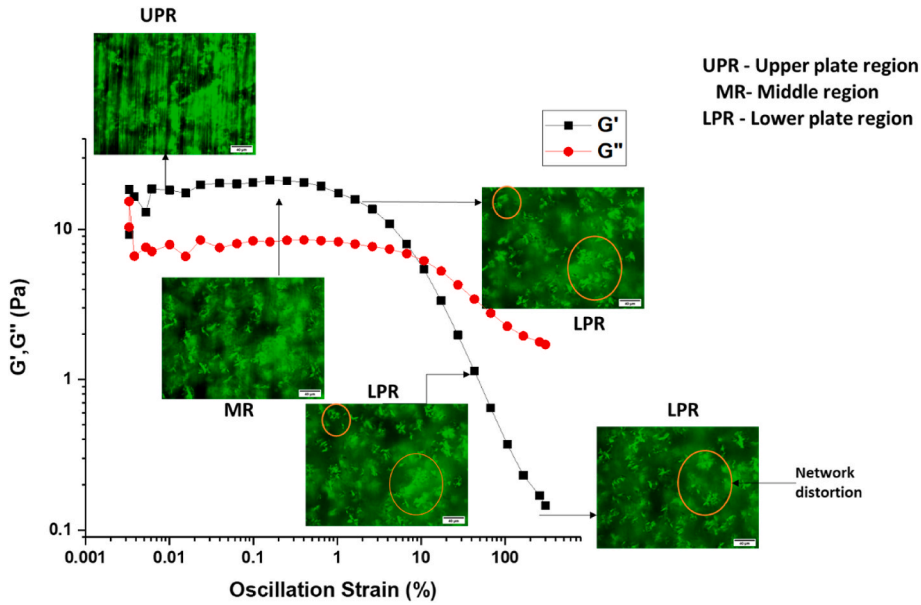

Fig. 7. In situ microscopy to CB + 1 wt% C (25) sample representing the amplitude sweep after 30 min at 22 °C. The videos during amplitude sweep are taken from the upper plate towards the lower plate; hence individual images with a change in crystal network with respect to the amplitude are marked with an orange zone. The scale bar = 40 μm. (For interpretation of the references to color in this figure legend, the reader is referred to the Web version of this article.)

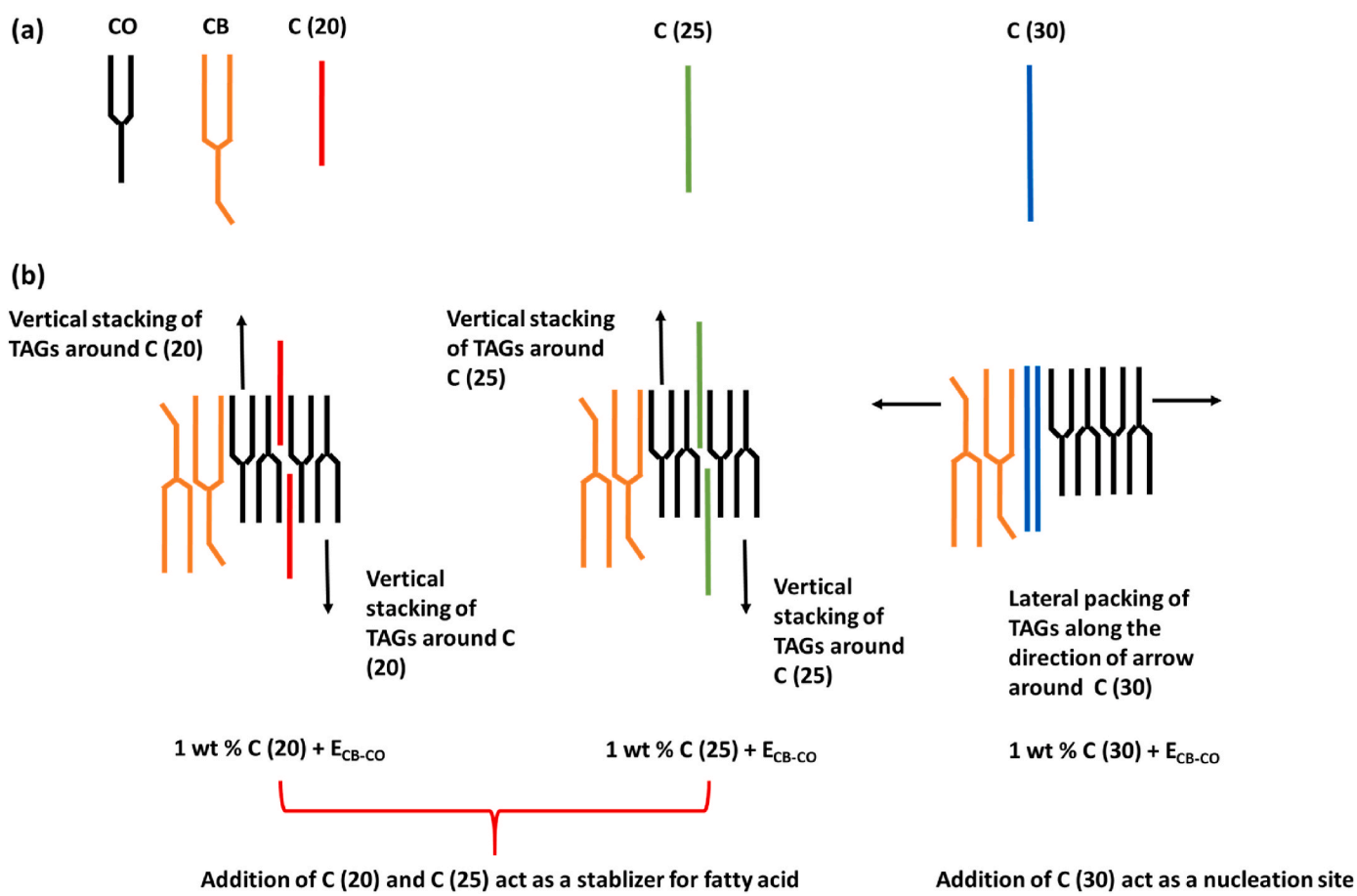

Fig. 8. Schematic representing possible interactions of CO and CB in eutectic mixture to C (20), C (25) and C (30).

multilayer arrangements of CO with C (20) occurs.

Additionally, the TAGs from CB arrange themselves in a vertical arrangement along with stacking of CO. However, the precise crystal domain arrangement is yet to be understood. Similar behavior with respect to the C (25) addition to the eutectic mixture is predicted according to the experimental results, whereas clear phase separation is

shown in case of C (30) addition. This schematic indicates that the addition of C (20) and C (25) stabilizes the fatty acids of a fat molecule, whereas C (30) addition act as a nucleation site.

Furthermore, the results emphasized that in the case of a eutectic mixture, n-alkanes acted as seed crystals with less concentration and provided a hint towards an organo-gelator role with more concentration (e.g., at and above 3 wt%) for a high number of carbon chain length (C (25) and C (30) with respect to models that are used). Further experiments with x-ray diffraction and rheology are of interest to understand in detail the interactions based on the unit cell of polymorphs, precise construction of ternary plot, and confirm the hypothesis of the formation of oleogel respectively. Thus, to conclude, although n-alkanes does not contribute to the food-grade system, the understanding of the interaction of these n-alkanes with CB and CO provides one step forward for deep insight into tailoring several products in confectionary application.

CRediT authorship contribution statement

Bhagyashri L. Joshi: Conceptualization, Methodology, Writing – original draft, Writing – review & editing, Data curation, Validation, Visualization. **Robert Graf:** Methodology, Writing – review & editing, Data curation, Validation, &, Visualization. **Sarah Gindra:** Methodology. **Thomas A. Vilgis:** Conceptualization, Writing – review & editing, Supervision, Validation, &, Visualization.

Declaration of competing interest

The authors declare that they have no known competing financial interests or personal relationships that could have appeared to influence the work reported in this paper.

Acknowledgment

The authors would like to thank Petra Räder for her contribution during the discussion of DSC experiments and to Andreas Hanewald for his assistance during rheology and rheo-microscopy experiments.

Appendix A. Supplementary data

Supplementary data to this article can be found online at https://doi.org/10.1016/j.crfs.2021.10.010.

References

Abdallah, D.J., Weiss, R.G., 2000. n-Alkanes gel n-alkanes (and many other organic liquids). Langmuir 16 (2), 352–355. https://doi.org/10.1021/la990795r.
Ali, A.R.M., Dimick, P.S., 1994. Melting and solidification characteristics of confectionery fats: anhydrous milk fat, cocoa butter and palm kernel stearin blends. J. Am. Oil Chem. Soc. 71 8, 803–806.
Avrami, M., 1941. Granulation, phase change, and microstructure kinetics of phase change. III. J. Chem. Phys. 9 (2), 177–184.
Avrami, M., 1940. Kinetics of phase change. II transformation-time relations for random distribution of nuclei. J. Chem. Phys. 8 (2), 212–224.
Avrami, M., 1939. Kinetics of phase change. I General theory. J. Chem. Phys. 7 (12), 1103–1112.
Blake, A.I., Co, E.D., Marangoni, A.G., 2014. Structure and physical properties of plant wax crystal networks and their relationship to oil binding capacity. J. Am. Oil Chem. Soc. 91 (6), 885–903.
Chaleepa, K., Szepes, A., Ulrich, J., 2010a. Effect of additives on isothermal crystallization kinetics and physical characteristics of coconut oil. Chem. Phys. Lipids 163 (4–5), 390–396.
Chaleepa, K., Szepes, A., Ulrich, J., 2010b. Effect of additives on isothermal crystallization kinetics and physical characteristics of coconut oil. Chem. Phys. Lipids 163 (4–5), 390–396. https://doi.org/10.1016/j.chemphyslip.2010.03.005.
Filippone, P.T., 2019. Paraffin Wax in Food This Edible Wax Adds Shine to Food. https://www.thespruceeats.com/what-is-paraffin-wax-1807043.
Freund, M., Csikos, R., Keszthelyi, S., Mozes, G., 1983. Paraffin Products, Properties, Technologies, Applications. Elsevier.
Geary, M., Hartel, R., 2017. Crystallization behavior and kinetics of chocolate-lauric fat blends and model systems. JAOCS, J. Am. Oil Chem. Soc. 94 (5), 683–692. https://doi.org/10.1007/s11746-017-2973-3.
Ishibashi, C., Hondoh, H., Ueno, S., 2017. Epitaxial growth of fat crystals on emulsifier crystals with different fatty acid moieties. Cryst. Growth Des. 17 (12), 6363–6371. https://doi.org/10.1021/acs.cgd.7b01039.
Jahurul, M.H.A., Zaidul, I.S.M., Norulaini, N.A.N., Sahena, F., Abedin, M.Z., Ghafoor, K., Omar, A.K.M., 2014. Characterization of crystallization and melting profiles of blends of mango seed fat and palm oil mid-fraction as cocoa butter replacers using differential scanning calorimetry and pulse nuclear magnetic resonance. Food Res. Int. 55, 103–109.
Joshi, B., Beccard, S., Vilgis, T.A., 2018. Fractals in crystallizing food systems. Curr. Opin. Food Sci. 21, 39–45.
Joshi, B.L., Zielbauer, B.I., Vilgis, T.A., 2020. Comparative study on mixing behavior of binary mixtures of cocoa butter/Tristearin (CB/TS) and cocoa butter/coconut oil (CB/CO). Foods 9 (3), 327.
Kamphuis, H., Jongschaap, R.J.J., 1985. The rheological behaviour of suspensions of fat particles in oil interpreted in terms of a transient-network model. Colloid Polym. Sci. 263 12, 1008–1024.
Lipp, M., Anklam, E., 1998. Review of cocoa butter and alternative fats for use in chocolate—Part B. Analytical approaches for identification and determination. Food Chem. 62 (1), 99–108.
Liu, C., Zheng, Z., Zaaboul, F., Cao, C., Huang, X., Liu, Y., 2019. Effects of wax concentration and carbon chain length on the structural modification of fat crystals. Food Funct 10 (9), 5413–5425.
Loisel, C., Keller, G., Lecq, G., Bourgaux, C., Ollivon, M., 1998. Phase transitions and polymorphism of cocoa butter. J. Am. Oil Chem. Soc. 75 (4), 425–439.
Marangoni, A.G., Wesdorp, L.H., 2012. Structure and Properties of Fat Crystal Networks. CRC Press.
Martini, S., Carelli, A.A., Lee, J., 2008. Effect of the addition of waxes on the crystallization behavior of anhydrous milk fat. J. Am. Oil Chem. Soc. 85 (12), 1097–1104.
Miskandar, M.S., Man, Y.B.C., Rahman, R.A., Aini, I.N., Yusoff, M.S.A., 2007. Effects of emulsifiers on crystal behavior of palm oil blends on slow crystallization. J. Food Lipids 14 (1), 1–18.
Quast, L.B., Luccas, V., Ribeiro, A.P.B., Cardoso, L.P., Kieckbusch, T.G., 2013. Physical properties of tempered mixtures of cocoa butter, CBR and CBS fats. Int. J. Food Sci. Technol. 48 (8), 1579–1588.
Ribeiro, A.P.B., Masuchi, M.H., Miyasaki, E.K., Domingues, M.A.F., Stroppa, V.L.Z., de Oliveira, G.M., Kieckbusch, T.G., 2015. Crystallization modifiers in lipid systems. J. Food Sci. Technol. 52 (7), 3925–3946.
Rothkopf, I., Danzl, W., 2015. Changes in chocolate crystallization are influenced by type and amount of introduced filling lipids. Eur. J. Lipid Sci. Technol. 117 11, 1714–1721.
Sangwal, K., 2007. Additives and Crystallization Processes: from Fundamentals to Applications. John Wiley & Sons.
Sato, K., 2018. Crystallization of Lipids, Fundamentals and Applications in Food, Cosmetics, and Pharmaceuticals, Crystallization of Lipids. John Wiley & Sons Ltd., West Sussex, UK https://doi.org/10.1002/9781118593882.
Stortz, T.A., Zetzl, A.K., Barbut, S., Cattaruzza, A., Marangoni, A.G., 2012. Edible oleogels in food products to help maximize health benefits and improve nutritional profiles. Lipid Technol. 24 (7), 151–154. https://doi.org/10.1002/lite.201200205.
Tran, T., Green, N.L., Rousseau, D., 2015. Spheroidal fat crystals: structure modification via use of emulsifiers. Cryst. Growth Des. 15 (11), 5406–5415.
Wille, R.L., Lutton, E.S., 1966. Polymorphism of cocoa butter. J. Am. Oil Chem. Soc. 43 (8), 491–496.
Williams, S.D., Ransom-Painter, K.L., Hartel, R.W., 1997. Mixtures of palm kernel oil with cocoa butter and milk fat in compound coatings. J. Am. Oil Chem. Soc. 74 (4), 357–366.
Wright, A.J., Hartel, R.W., Narine, S.S., Marangoni, A.G., 2000. The effect of minor components on milk fat crystallization. J. Am. Oil Chem. Soc. 77 (5), 463–475.
Zhang, L., Chen, F., Zhang, P., Lai, S., Yang, H., 2017. Influence of rice bran wax coating on the physicochemical properties and pectin nanostructure of cherry tomatoes. Food Bioprocess Technol. 10 (2), 349–357.
Zulim Botega, D.C., Marangoni, A.G., Smith, A.K., Goff, H.D., 2013. The potential application of rice bran wax oleogel to replace solid fat and enhance unsaturated fat content in ice cream. J. Food Sci. 78 (9), C1334–C1339.